High fidelity data generation and fault diagnosis of a gear pump

Kayal Lakshmanan[1], Fabrizio Tessicini[2], Antonio J. Gil[1], Ferdinando Auricchio[3]

[1] *Faculty of Science and Engineering Swansea University Swansea, UK*
k.lakshmanan@swansea.ac.uk
[2] *Innovation Head F-Lab Milano, Italy*
[3] *Department of Civil Engineering and Architecture University of Pavia Pavia, Italy*

Abstract

The sudden failure of industrial components can adversely affect an organisation regarding time, cost, and workflow. To prevent downtime that could result in a major disruption, it is crucial to keep equipment components in optimal condition. Hence developing a system that can detect an equipment failure early is essential. The present work proposes a computational strategy of fault diagnosis using Machine Learning (ML) algorithms for an external gear pump. Due to the lack of sufficient experimental data, a novel approach of creating a high-fidelity in-silico data using a Computational Fluid Dynamic (CFD) model of the gear pump in both normal and defective working conditions (viscosity variations, radial gap variations, speed variations, etc.) is introduced. A novel synthetic data generation technique is implemented by perturbing the frequency content of the time series to recreate other working conditions. These synthetically generated datasets are used to train the underlying ML metamodel. Three different ML classification algorithms are used for fault diagnosis, namely Multilayer Perceptron (MLP), Naive Bayes (NB),and Support Vector Machine (SVM).

River Journal, 1–16.

1 Introduction

Gear pumps are comprised of sophisticated gear arrangements used to pump fluid under a variety of working conditions. For example, the Fluid-o-tech external gear pump has been used within medical equipment, ink-jet printing systems, cooling systems, sanitisation applications, etc. [1]. Due to a sophisticated and compact design, external gear pumps can be easily fit inside complex industry equipment reducing the manufacturing time and associated cost. However, the sudden failure of any industry component can have negative consequences on the industry in terms of time and workflow. As a result, Predictive Maintenance has emerged as a necessary tool to predict failure and minimise industrial downtime and associated cost. Predictive Maintenance techniques help determine the condition of in-service equipment to predict when maintenance should be performed. It is crucial to monitor the actual mechanical condition of the machine's health regularly to avoid sudden failure.

In order to perform fault diagnosis using data-driven approaches, the actual condition of the gear pump needs to be monitored. Additionally, the availability of a sizable collection of high-fidelity data is crucial for ML predictive capabilities [2]. High-fidelity in-silico data can be used to replace experimental data in cases where it is unavailable or not sufficient [3, 4]. In this work, the gear pump operations are accurately modelled using a CFD model that can simulate both normal and varied fault cases such as radial gap variations, clogging, viscosity variations, etc. From these simulations, pressure, flow rate, and torque are monitored for several working conditions of the pump.

A noise perturbation method is introduced by increasing noise function in specific frequency components monotonically to reproduce potential environmental fluctuations of the working pump from the in-silico data [5, 6]. Finally, the synthetically generated datasets are used to extract the features that will eventually be used to train an ML model.

The nearest neighbour algorithm, SVM, probabilistic-based algorithms like the Bayesian network, and Naive Bayes are traditionally used for fault detection [7]. Currently, Artificial Neural Networks, fuzzy–neural networks, evolutionary algorithms, and deep learning algorithms are widely used ML techniques for fault diagnosis [8, 9, 10]. The recurrent neural network and the convolutional neural network models have demonstrated enhanced performance over time in the field of fault diagnostics [11, 12, 13, 14].

This industry-academia collaboration sought to address one specific bottleneck: finding an efficient strategy to create a reliable dataset with the same properties of the real-world data and perform fault diagnosis of the external gear pump with insufficient availability of experimental data. As a result, this work has proposed a fault diagnosis methodology using supervised learning ML algorithms MLP, SVM and NB and synthetic data generation methods to support ML algorithms.

Following the introduction, Section 2 introduces the generation of high-fidelity in silico data using a Computational Fluid Dynamics (CFD) model of a gear pump, Section 3 describes the synthetic generation method, Section 4 presents the framework fault diagnosis, and Section 5 summarises the conclusions.

2 Generation of High-fidelity data using Computational fluid dynamics simulation of an external gear pump

The CFD model is developed utilising the commercial code 'Simerics MP+' that numerically solves the mass, momentum, and energy conservation equations. Also incorporates precise physical models for turbulence and cavitation. The mathematical model and governing equations are detailed in [15].

2.1 Geometry

Gear pumps are rotating positive displacement external gear pumps, where the fluid is displaced from the inlet side of the pump to the outlet side of the pump due to the intermeshing of the drive and the slave gear's teeth. The geometry of the external gear pump, which is of main interest to this work, is shown in Figure 1. However, some specific geometry features have been hidden due to commercial sensitivity.

The lubrication channel is connected to the gears through the top channel with rotating shafts, and the gears are sealed inside a tight, leak-free housing. Likewise, a bottom channel with rotating shafts connects the rear side of the gear to the magnet. The inlet and outlet ports are connected to the sides of the gear. The inlet and outlet sensors are placed in the inlet and outlet ports. The outlet sensor is placed away from the end to avoid reversing the flow and accurately measure the pressure distribution in the outlet port. During the operation, these types of pumps are noiseless, pulsation-free and capable of

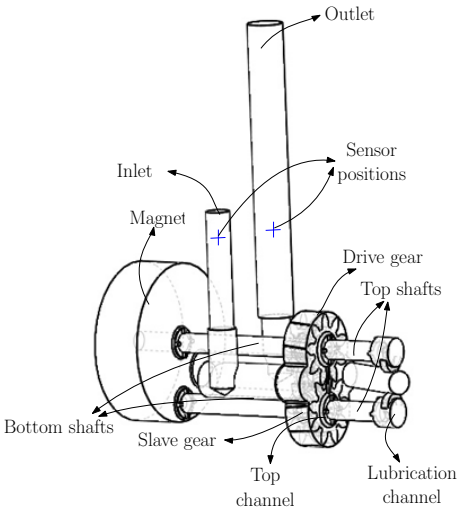

Figure 1 Geometry of the external gear pump. Specific features of the geometry and the measurements have been hidden due to commercial sensitivity.

handling liquids up to 95 °C with pressure up to 12 bar and flow rate up to 210 l/h [1].

2.2 Model attributes

The fluid domain of the external gear pump is extracted from the Computer-Aided Design (CAD) of the pump, which is provided by the industrial partner F-Lab and the geometry is imported into Simerics MP+. For extremely curved sections or narrow cut portions, high-quality hexahedral cells are produced using the binary tree unstructured mesh. Additionally, Simerics MP+ features a specialised tool for meshing the interior geometry of the gear using a rotor gear template mesh, resulting in highly structured hexahedral cells of excellent quality [16]. The entire fluid domain's mesh is created utilising Simerics MP+ with 446393 cells (see Figure 2). High-quality hexahedral cells are generated using the unstructured mesh for high-curved or narrowly cut sections, such as shafts and magnets.

The simulation of an external gear pump running in healthy conditions use the conditions presented in Table 2.2. The boundary condition for the inlet pressure is atmospheric pressure and for the outlet is 3.15 bar.

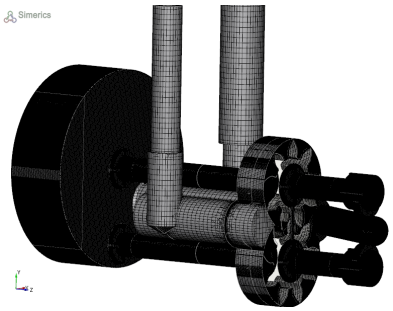

Figure 2 Mesh of the external gear pump (the entire fluid domain) created using Simerics MP+.

Table 1 Properties of a healthy (normal working condition) gear pump.

Operating conditions of the gear pump	
Speed	1450 rpm
Radial gap	0.03 mm
Number of drive gear teeth	9
Number of slave gear teeth	9
Material properties of the gear pump	
Viscosity	0.0383 Pa-s
Density	800 kg/m^3
Temperature	300 K

2.2.1 Mesh sensitivity analysis

A mesh sensitivity analysis is carried out, whereby a finer and finer mesh is used until a threshold of accuracy is passed going from one model to the next [17]. For simplicity and to optimise the number of cells, a simpler geometry is considered with the inlet port, the outlet port, and external gear in Figure 1. Simulations are performed for fixed time step with four different grid sizes (h_1, h_2, h_3, h_4) ranging from coarse to fine mesh. The properties of different grid sizes and their commutation time are displayed in Table 2. Figure 3 illustrates the relative error percentage of pressure, flow rate, and torque at a fixed time step for the various cell counts, and it can be seen that the relative error reduces as the cell count increases. Due to the effectiveness of the Simerics MP+, even though the discretisation accuracy in the case of the h3 mesh is of first order, the accuracy of the solution is above second order. As an outcome of this investigation, all CFD analyses are carried out using mesh size h3.

Table 2 Mesh sensitivity analysis: execution time is in a dimensionless quantity, where h_1 is used as reference.

	h_1	h_2	h_3	h_4
No of elements	44518	247495	446393	4605699
Max cell size	0.1	0.07	0.03	0.018
Min cell size	0.005	0.005	0.002	0.001
Execution time	1	3.24	7.57	182.76

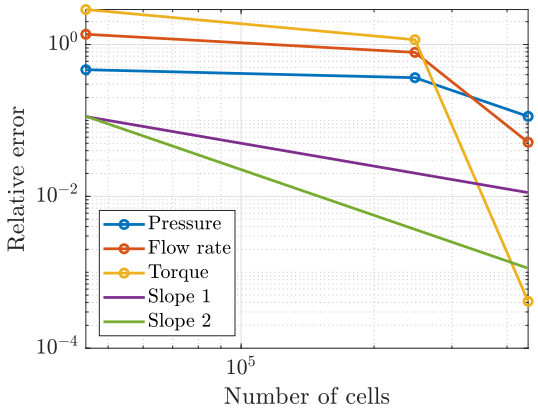

Figure 3 Relative error of pressure, flow rate and torque (fixed time step) in relation to finest mesh (h_4).

2.3 CFD model validation against experimental data

To validate the CFD model, our industrial partner provided the experimental results of the external gear pump (Figure 1) with the exact specifications mentioned in Section 2.2. The gear pump experiment was carried out by setting speed and viscosity levels for various outlet pressure values from 1 to 9 bar. The inlet pressure is assumed to be atmospheric pressure (1.01325 bar) for all the experiments. The discharge flow rate has been measured for each experiment, and the average of these values has been used to validate the CFD model. Particularly, the investigations were performed out for the gear's two distinct rotational speed values, 1450 rpm and 2900 rpm. For the 1450 rpm speed, two different viscosity values, 0.001 Pa-s and 0.075 Pa-s and for the 2900 rpm, three different viscosity values, 0.001 Pa-s, 0.02 Pa-s and 0.075 Pa-s are considered. CFD simulations with the healthy scenario, different speed scenarios, and different viscosity scenarios are validated against experimental

values. The following results are standardised using standardisation or z-score normalisation technique for the confidentiality purpose. Standardisation is expressed as $\boldsymbol{x} - \mu/\sigma$, where $\boldsymbol{x}$ is data vector and μ and σ is mean and standard deviation of $\boldsymbol{x}$.

Figure 4 compares the standardised average experimental outlet flow rate of a gear pump with a rotating speed of 1450 rpm to the CFD simulation models for various pressure levels and two different viscosity levels of 0.001 Pa-s and 0.075 Pa-s. The relative pressure, that is, the difference between outlet and inlet pressure values are shown in x-axis. Figure 5 compares the standardised average experimental outlet flow rate of a gear pump with a rotating speed of 2900 rpm to the CFD simulation models for various pressure levels and two different viscosity levels of 0.001 Pa-s and 0.075 Pa-s. From Figures 4 and 5, it can be seen that the simulation results are in very good agreement with experiments. Additionally, a greater viscosity value leads to a high discharge flow rate.

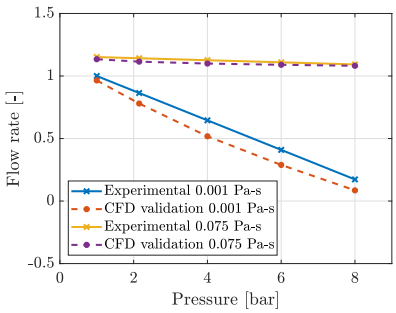

Figure 4 Standardised average outlet flow rate of experimental results against CFD model of gear pump with speed of 1450 rpm for different relative pressure values.

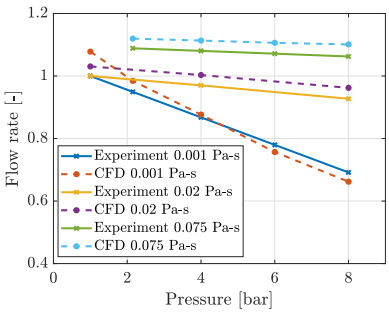

Figure 5 Standardised average outlet flow rate of experimental results against CFD model of gear pump with speed of 2900 rpm for different relative pressure values.

2.4 Implementation of fault conditions in the external gear pump

After validating various viscosity values and two different speed values in the CFD simulations with experimental values, we have built potential fault scenarios which can cause the pump to degrade or even fail. The fault scenarios are built to understand the pump's complete behaviour when running in an abnormal condition. Finally, various working conditions are recreated based on the validated CFD models and the experience of the industrial partner, including, radial gap degradation, axial gap degradation, speed variations(validated

experimentally), viscosity variations(validated experimentally), temperature variations and clogging (or blocking) variations, as depicted in Figure 6.

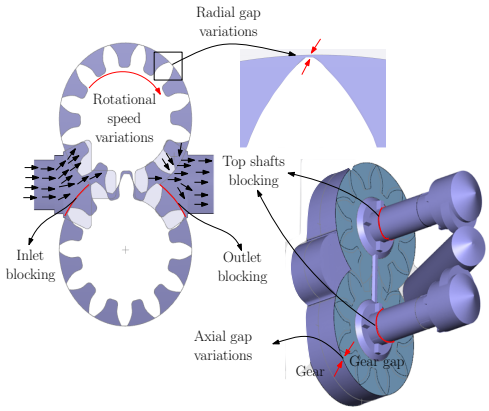

Figure 6 Developed fault scenarios using the gear pump's normal operating state as a benchmark.

The fault variables and their various cases (in percentage) are displayed in Table 2.4. The percentage is calculated considering the healthy working conditions parameters of the gear pump as a reference. Following Section 2.2, all fault scenarios are simulated.

Table 3 Implemented fault scenarios; the percentage is calculated considering healthy working conditions parameters of gear pump as reference.

Fault scenarios	Different cases
Radial gap degradation (G)	66.66%, 133.33%, 200%
Axial gap degradation (A)	2.5%, 5%, 7.5%
Speed variations (S)	1.78%, 3.57%, 5%
Viscosity variations (V)	0.8%, 1.6%, 2.4%
Temperature variations (T)	2.5%, 5%, 7.5%
Clogging variations (C)	blocked inlet, outlet, top shafts

For all cases, the gear pump is run for five gear revolutions (1450 rpm) with an atmospheric (1.01325 bar) inlet pressure and outlet pressure of 3.15 bar. The first revolution is for the initialisation of flow, and the second to fifth revolution is considered for the results. For data acquisition, pressure at the outlet sensor (sensor shown in Figure 1), the discharge flow rate and the sum of drive and slave gear's torque have been considered primary sensor variables.

For instance, fault scenarios due to radial gap degradation are created based on the concept that mass particles can enter the pump, causing the gear teeth and the gear case to erode, as displayed in Figure 6. In our work, the radial gap faults are generated by increasing the gap between the gear and the gear case and re-running appropriate CFD simulations. Step-by-step degradation behaviour is generated, namely G1, G2 and G3, to understand the erosion behaviour between the gear teeth and gear case. The standardised discharge flow rate of the scenarios (G1, G2, G3) compared with the healthy scenario (H) is shown in Figure 7. The mean flow rate of G1, G2 and G3 is decreased by 21%, 40% and 56%, respectively, concerning the healthy scenario; this concludes that increasing the gap size decreases the mean flow rate.

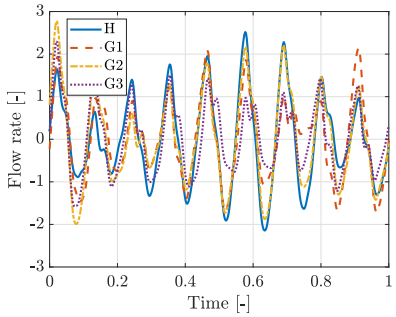

Figure 7 Discharge flow rate with respect to time of radial gap fault scenarios.

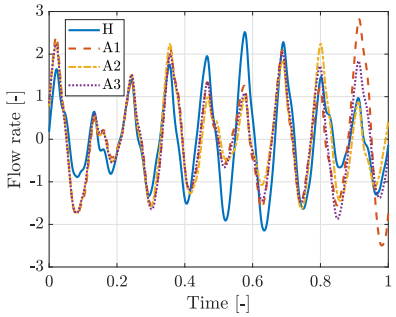

Figure 8 Discharge flow rate with respect to the time of axial gap fault scenarios.

The axial gap degradation are designed to understand the impact of flow leakage inside the fluid volume. They are produced by widening the axial gap (side leakage) between the gear and the gear perimeter without moving the gear centre, as shown in 6. Similar to radial gap fault scenarios, the discharge flow rate decreases with the incremental increase of axial gap size. The standardised discharge flow rate of scenarios (A1, A2, A3) compared with the healthy scenario (H) is shown in Figure 8. Comparing to the healthy scenario, the mean flow rate of axial gap variations (A1, A2 and A3) is decreased by 2%, 4% and 6.3%, respectively.

The fault scenarios due to speed variations are introduced by increasing the rotational speed (in RPM) of the gear pump to find out the flow behaviour. The speed variations are created to validate that for positive displacement pumps, as the rotational speed increases, the discharge flow rate increases in linear trend, which is proven in [16] for an external gear pump. The step-by-

step increase in speed variations (S1, S2 and S3) increases the mean flow rate by 2%, 4.5% and 6.3%, respectively, concerning the healthy scenario.

The fault scenarios due to viscosity variations are produced to learn the pump's flow performance in the change of viscosity values. Gear pumps are best suitable for high viscosity applications. When the fluid viscosity decreases, slip increases; the slip is when the pump recirculates from the outlet to the inlet side as it escapes through machined clearances while the pump tries to progress forward. The amount of slip is determined by the fluid's viscosity and discharge pressure. A thin fluid with a low viscosity can squeeze through the clearances more easily than thicker fluids, where high discharge pressure can force thinner fluids back through the pump, causing more slipping. Because thin fluids slip, the pump's efficiency decreases as less product progress with the forward movement, hence the lower discharge flow rate. As a result, the mean flow rate of viscosity variations (V1, V2 and V3) is increased by 0.4%, 1% and 1.5%, respectively, compared to the healthy scenario.

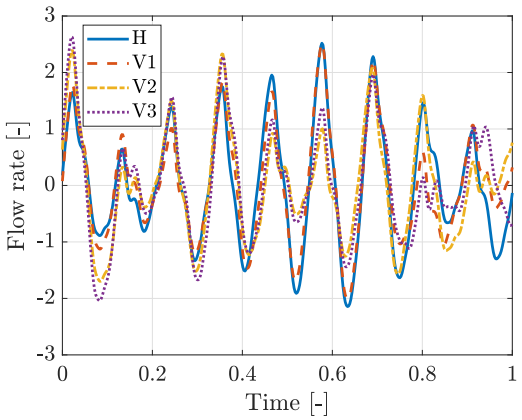

Figure 9 Discharge flow rate with respect to the time of radial gap fault scenarios.

The fault scenarios due to temperature variations are generated to comprehend the changes in the gear pump's performance with respect to temperature variations. An increase in temperature heats up the fluid transported through the pump, which reduces the fluid viscosity. As discussed above, an increase in viscosity increases the discharge flow rate. So, due to an increase in temperature, the viscosity decreases, which implies that the discharge flow rate decreases. Considering the healthy scenario, the mean flow rate of temper-

ature variations (T1, T2 and T3) is decreased by 0.16%, 0.25% and 0.33%, respectively.

The fault scenarios due to clogging or blocking are implemented to validate the sudden disturbances due to any blockages in the pump. For this reason, various parts of the pump, the outlet (C1), the inlet (C2) and the top shafts (C3), are partially blocked. The CFD simulation is performed, and the discharge flow rate can be measured. Blocking a part of the outlet (C1) and part of the inlet (C2), the discharge flow rate is decreased by 4% and 0.5%, and however, when blocking the top shafts (C3), the discharge flow rate is increased by 0.19%.

The results of the faulty scenarios are extracted in time series, which will be used perform the fault diagnosis in Section 4.

3 Synthetic data generation method for fault diagnosis using a noise perturbation method

A large amount of data is a prerequisite for any ML algorithm in order to better the learning phase. Using a noise perturbation method, the high-fidelity data generated by the CFD model is modified to simulate potential environmental fluctuations of the working pump settings. The addition of noise is carried out by perturbing the frequency content by an error function constructed in the following manner

$$\hat{x}^{mod}(\tilde{\omega_j}) = \hat{x}(\tilde{\omega_j})[1 + \alpha\epsilon(\tilde{\omega_j})] \tag{1}$$

where $\hat{x}(\tilde{\omega_j})$ is the original frequency content (for a selected frequency ω_j) obtained from a discrete Fourier transform, α is a scalar parameter tuned depending on the amount of noise added and $\epsilon(\omega_j)$ is a monotonically increasing function of the frequency ω (larger noise added in larger frequencies).

4 Fault diagnosis results

The present section presents a fault diagnosis (fault detection) of the external gear pump by means of the three alternative ML algorithms, namely MLP, SVM and NB. The overview of the designed fault diagnosis simulation process is depicted in Figure 10.

The availability of huge collections of high-fidelity data is essential for ML predictive performance [2]. In case of limited experimental data avail-

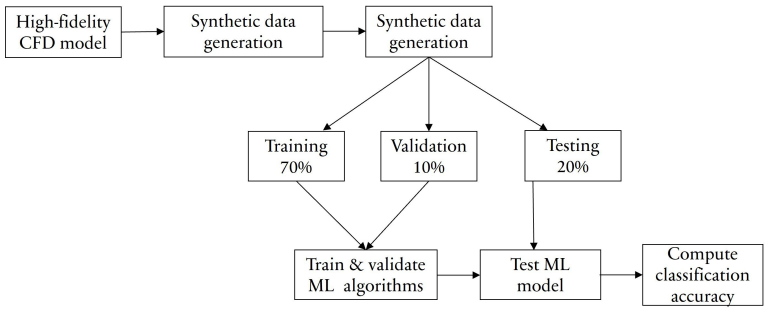

Figure 10 Overview process of fault diagnosis using ML classification algorithms.

ability (or absence), these can be superseded using high-fidelity in-silico data. The aspect of high-fidelity data generation has been discussed in Section 2. Large volumes of data are typically required to improve any ML algorithm's predicted response. A synthetic data generation method is implemented to facilitate the gathering of data greatly (see Section 3).

Once the dataset is gathered, it is divided into a training dataset (used to fit the model) comprised of 70%, validation comprised of 10%, and a test dataset (used to provide an unbiased evaluation of a final model fit on the training dataset) comprised of the remaining 20% randomly. The training dataset is used to train each ML algorithm, which is tested against the test dataset, and the accuracy of the model is computed. In this work, the optimisation of these hyper-parameters is performed using a random search for all the methods.

For this example, we consider the healthy dataset (H) and all six types of fault scenarios implemented with 18 different cases (C1, C2, C3, G1, G2, G3, S1, S2, S3, T1, T2, T3, W1, W2, W3 V1, V2, V3). Variables such as pressure, flow rate and torque are monitored for all the fault scenarios. These datasets are in the form of a discrete set of time values. The synthetic data generation approach is used to increase the availability of data needed to train the ML approach. The generated datasets are standardised and used as input datasets for training and testing ML algorithms. The output data is considered as labels (H, C1, C2,...V2, V3). The training dataset is trained using MLP, SVM and NB and tested against the test dataset, where the accuracy of the test dataset is calculated between model output and desired output. Following the overview designed process of fault diagnosis in Figure 10, a fault diagnosis is performed for the desired dataset.

The backpropagation technique is employed for the training of the MLP network to optimise the updating of the weights in accordance with the loss

function given during model development. The backpropagation algorithm requires that the network is trained for a specified number of epochs to the training dataset. Each epoch can be partitioned into groups called batches. The batch size determines how many patterns the network is exposed to in a single epoch before the weights are adjusted. The model loss is typically displayed in relation to the number of epochs. This plot can detect if the model is overfitting, underfitting or suitably fitting to the training dataset [18]. Furthermore, the Early Stopping Argument is utilised to terminate the training when the selected performance metric reaches a point of no further improvement [19]. For SVM classification, three hyper-parameters are considered: kernel function, kernel parameter, and regularisation parameter. A random search algorithm is utilised to ensure the optimal choice of hyper-parameters for SVM.

Table 4 Classification accuracy of pressure, flow rate and torque using MLP, SVM and NB.

	MLP	SVM	NB
Pressure	100.0 %	99.12 %	99.28 %
Flow rate	100.0 %	97.42 %	94.75 %
Torque	98.23 %	94.64 %	69.92 %

Table 4 shows the classification test accuracy of pressure, flow rate and torque using ML algorithms MLP, SVM and NB. The accuracy obtained using ML algorithms, compared to pressure and flow rate, torque provides relatively lower accuracy. In contrast, the use of a flow rate provides the highest fault diagnosis accuracy. Moreover, for almost all cases, the classification accuracy is high due to the discrete information of various fault cases, however, torque suffers from comparatively low accuracy with all three ML algorithms, especially with NB.

5 Conclusion and remarks

This paper has presented a novel methodology for fault diagnosis using Machine Learning (ML) algorithms for an external gear pump. In this regard, the main novelty of this work is the generation of high-fidelity data for the external gear pump, using CFD models and synthetic data generation methods, and a framework for a fault diagnosis strategy with the application of ML algorithms.

In-silico data generation techniques offer a long-term resolution to limited or missing experimental data and provide additional investigation through ML or other data analysis techniques. Moreover, the synthetic data generation method can be employed where data privacy can be of significant concern. Fault diagnosis of the gear pump has been performed using feature extraction methods and three types of ML classification algorithms: MLP, SVM, and NB.

The engineering sector is primarily interested in finding affordable ways to do these assessments. This would suggest the use of the torque as the magnitude to be most easily monitored because it is linearly related to current absorption, which can be monitored via the current sensor. Hence, torque analysis is performed for fault diagnosis. However, compared to pressure and flow rate, torque provides comparatively lower classification accuracy, which results in the question of accuracy versus cost. If the industry chooses to use torque to perform fault diagnosis, then there is a trade between the cost and accuracy.

References

[1] Fluid-o-tech. URL `https://www.fluidotech.it/en/products/technologies/external-gea` Accessed: 2021-04-03.

[2] Ziad Obermeyer and Ezekiel J Emanuel. Predicting the future—big data, machine learning, and clinical medicine. *The New England journal of medicine*, 375(13):1216, 2016.

[3] Yaomin Zhao, Harshal D Akolekar, Jack Weatheritt, Vittorio Michelassi, and Richard D Sandberg. Rans turbulence model development using cfd-driven machine learning. *Journal of Computational Physics*, 411: 109413, 2020.

[4] Faria T Zahura, Jonathan L Goodall, Jeffrey M Sadler, Yawen Shen, Mohamed M Morsy, and Madhur Behl. Training machine learning surrogate models from a high-fidelity physics-based model: Application for real-time street-scale flood prediction in an urban coastal community. *Water Resources Research*, 56(10):e2019WR027038, 2020.

[5] Kayalvizhi Lakshmanan, Antonio J Gil, Ferdinando Auricchio, and Fabrizio Tessicini. A fault diagnosis methodology for an external gear pump

with the use of machine learning classification algorithms: Support vector machine and multilayer perceptron. Loughborough University, 2020. doi: https://doi.org/10.17028/rd.lboro.12097668.v1.

[6] Kayal Lakshmanan, Fabrizio Tessicini, Antonio J Gil, and Ferdinando Auricchio. A fault prognosis strategy for an external gear pump using machine learning algorithms and synthetic data generation methods. *Applied Mathematical Modelling*, 123:348–372, 2023.

[7] B Samanta. Gear fault detection using artificial neural networks and support vector machines with genetic algorithms. *Mechanical systems and signal processing*, 18(3):625–644, 2004.

[8] Arfat Siddique, GS Yadava, and Bhim Singh. Applications of artificial intelligence techniques for induction machine stator fault diagnostics. In *4th IEEE International Symposium on Diagnostics for Electric Machines, Power Electronics and Drives, 2003. SDEMPED 2003*, pages 29–34. IEEE, 2003.

[9] Matheus F Torquato, Kayal Lakshmanan, Natalia Narożańska, Ryan Potter, Alexander Williams, Fawzi Belblidia, Ashraf A Fahmy, and Johann Sienz. Cascade optimisation of battery electric vehicle powertrains. *Procedia Computer Science*, 192:592–601, 2021.

[10] Kayal Lakshmanan, Eugenio Borghini, Arnold Beckmann, Cameron Pleydell-Pearce, and Cinzia Giannetti. Data modelling and remaining useful life estimation of rolls in a steel making cold rolling process. *Procedia Computer Science*, 207:1057–1066, 2022.

[11] Dawei W Dong, John J Hopfield, and KP Unnikrishnan. Neural networks for engine fault diagnostics. In *Neural Networks for Signal Processing VII. Proceedings of the 1997 IEEE Signal Processing Society Workshop*, pages 636–644. IEEE, 1997.

[12] C James Li and Tung-Yung Huang. Automatic structure and parameter training methods for modeling of mechanical systems by recurrent neural networks. *Applied Mathematical Modelling*, 23(12):933–944, 1999.

[13] Roberto M Souza, Erick GS Nascimento, Ubatan A Miranda, Wenisten JD Silva, and Herman A Lepikson. Deep learning for diagnosis and

classification of faults in industrial rotating machinery. *Computers & Industrial Engineering*, 153:107060, 2021.

[14] Kayal Lakshmanan, Davide Balatti, Hamed Haddad Khodaparast, Michael I Friswell, and Andrea Castrichini. Experimental and numerical gust identification using deep learning models. *Applied Mathematical Modelling*, 132:41–56, 2024.

[15] Hui Ding, FC Visser, Y Jiang, and M Furmanczyk. Demonstration and validation of a 3d cfd simulation tool predicting pump performance and cavitation for industrial applications. *Journal of fluids engineering*, 133 (1), 2011.

[16] Feng Qi, Sujan Dhar, Varun Haresh Nichani, Chiranth Srinivasan, De Ming Wang, Liang Yang, Zhonghui Bing, and Jinming Jim Yang. A cfd study of an electronic hydraulic power steering helical external gear pump: Model development, validation and application. *SAE International Journal of Passenger Cars-Mechanical Systems*, 9(2016-01-1376):346–352, 2016.

[17] Wu-Gui Jiang, Ren-Zhi Zhong, Qing H Qin, and Yong-Gang Tong. Homogenized finite element analysis on effective elastoplastic mechanical behaviors of composite with imperfect interfaces. *International journal of molecular sciences*, 15(12):23389–23407, 2014.

[18] Koushal Kumar and B Abhishek. *Artificial neural networks for diagnosis of kidney stones disease*. GRIN Verlag, 2012.

[19] François Chollet et al. Keras, 2015. URL `https://keras.io`. Accessed: 2020-09-06.